Influence of Organophilic Montmorillonite and Polypropylene on the Rheological Behaviors and Mechanical Properties of Ultrahigh Molecular Weight Polyethylene

Jinggang Gai, Huilin Li

State Key Laboratory of Polymer Materials Engineering, Polymer Research Institute of Sichuan University, Chengdu, Sichuan 610065, People's Republic of China

Received 23 October 2006; accepted 26 December 2006
DOI 10.1002/app.26112
Published online 12 April 2007 in Wiley InterScience (www.interscience.wiley.com).

ABSTRACT: The effects of organophilic montmorillonite (OM)/poly(ethylene glycol) (PEG) hybrids and polypropylene (PP) on the phase morphology, rheological behaviors, and mechanical properties of ultrahigh molecular weight polyethylene (UHMWPE) were investigated. The presence of the OM/PEG hybrids and PP in UHMWPE was found that it was able to lead to a significant reduction of melt viscosity and enhancement in tensile strength, and elongation at break of UHMWPE. A quantitative analysis indicated a larger affinity of the OM to the PEG than to PP or UHMWPE in the composites, suggesting that OM was intercalated by PEG. This was proposed to be responsible for the reduction of viscosity. Polarizing optical microscopy analysis, on the other hand, indicated that the dispersed OM, which acted as a nucleating agent, lowered the spherulite dimension and increased the spherulite number, resulting in high tensile strength and elongation at break. J Appl Polym Sci 105: 1200–1209, 2007

Key words: polypropylene; polyethylene; composite; morphology

INTRODUCTION

Ultrahigh molecular weight polyethylene (UHMWPE) was chosen for this study because it exhibits a number of desirable chemical and mechanical characteristics, including high tensile and impact strength, good chemical resistance, and excellent wear properties.[1,2] Its application, however, is limited due to its poor processability.

In the last 25 years, the development of high-performance UHMWPE composites has been well established in industry and academia, and often involved the use of a low molecular weight solvent to reduce the high entanglement density in forming the final products. The apparent disadvantage of such processes is the use of organic solvents, which are difficult to recycle and to remove. Alternative route of its modification by incorporation of a second polymer, an intermediate molecular weight polyethylene for example, indeed could improve the melt processability of UHMWPE. It is, however, not without an attendant disadvantage in the process as effective amounts of intermediate molecular weight polyethylene causes a remarkable decrease in some of the most desirable properties. For example, the original excellent mechanical properties are not easy to maintain.

Recently, mixtures of polymers and layered smectite clays have been prepared with significantly enhanced solid-state mechanical, dimensional, permeability, and flame-retardant properties[3,4] relative to the pure polymer. These enhancements have been achieved at low clay particle loadings, typically in the range 1–10 wt %. It has been hypothesized that large surface area, high aspect ratio, and good interfacial interaction are essential to produce enhanced solid-state properties in composites materials.[5] Thus, the optimal nanocomposite structure is thought to consist of disordered, exfoliated clay platelets dispersed in a polymer matrix.

The desired clay morphology has been accomplished by the melt mixing method. Natural clay is hydrophilic, and the polymer in which natural clay is to be dispersed is often hydrophobic. Thus, surfactants, typically aliphatic amines are introduced in the gallery regions between the clay layers by means of cation exchange. This process renders the clay

Correspondence to: H. Li (nic7703@scu.edu.cn).
Contract grant sponsor: National Nature Science Foundation of China; contract grant number: 50233010.
Contract grant sponsor: National Basic Research Program of China; contract grant number: 2005CB623800.
Contract grant sponsor: Foundation of Doctoral Disciplines, Ministry of Education of China; contract grant number: 20030610057.

more hydrophobic. The intercalated amine species thereby improve compatibility with the polymeric host while also increasing the clay layer interlayer spacing. Increased intercalation and exfoliation will occur if the organophilic clay possesses sufficient affinity for the host and the additive. Polypropylene (PP) and poly(ethylene oxide) clay hybrids have all been prepared by melt mixing.[6–8] Most attention has been paid to the mechanical properties of nanocomposites while only a few investigations have reported their rheological behaviors.[9,10]

In this article, the effects of UHMWPE/PP weight ratio, hybrids organophilic montmorillonite (OM)/ poly(ethylene glycol) (PEG) weight ratio and content on the phase morphology, rheological behaviors and mechanical properties of UHMWPE composites have been investigated. The possible mechanisms of enhancement in mechanical properties and reduction of melt viscosity have been proposed.

EXPERIMENTAL

Materials

Ultrahigh molecular weight polyethylene (UHMWPE) (M-II), with an average viscosity molecular weight of 2.5×10^6 and a mean particle diameter of about 300 μm, was supplied by Beijing No. 2 Auxiliary Agent Factory (Beijing, China). Poly(ethylene glycol) (PEG) was supplied by Liaoyang Aoke Chemical Co. (Liaoning, China) with a molecular weight of 6000. Polypropylene (PP) (F401) was supplied from Lanzhou Chemical Industry Factory (Lanzhou, China) with a melt flow rate (MFR) of 2.0 g/10 min (230°C, 2.16 kg load). Organophilic montmorillonite (OM) named DK-1 was supplied by Zhejiang Fenghong clay Chemicals Co. (Zhejiang, China) with a BET surface area of 150 m^2/g. DK-1 is a natural montmorillonite modified with hexadeoyltrimethylammonium chloride.

Sample preparation

PEG was first added to alcohol to form a uniform solution. The as-received OM powders were subsequently added to the uniform solution. The mixture was then heated to 60°C for 3 h and under vigorous stirring and formed a homogeneous suspension. The OM/PEG hybrids (MP) were dried in a 50°C oven for 4 days and then pulverized. The OM/PEG with weight ratio 1 : 1, 1 : 2, and 2 : 1 were donated as MP11, MP12, and MP21, respectively.

The addition of MP was 1–5 parts per hundred parts of UHMWPE/PP (phr) by weight. UHMWPE was physically mixed with PP and MP, then extruded by a general three-section single-screw extruder (D = 20 mm, L/D = 25). The temperatures were 190, 210, and 220°C for each section of the barrel and 210°C for the die. The extrudates were then made into pellets and compression molded into 1 and 4 mm plates. Compression molding was carried out in the following conditions: preheated at 200°C for 5 min at low pressure, compressed for 5 min at 13 MPa at the same temperature, and then cooled to ambient temperature with the cooling rate 30°C/min in the mold at 13 MPa. Specimens for tensile test or izod-notched impact tests were got from the 1 and 4 mm plates, respectively.

Mechanical properties

Tensile tests were carried out at room temperature according to GB/T 1040-92 standard on Instron model 4302 machine (Instron Co., Birmingham, UK). Modulus and elongation at break were measured at a cross-head speed of 50 mm/min. Notched izod impact strength was measured with XJ-40AX (Wuzhong Material Testing Technical Co., China) at room temperature according to GB 1843-80 standard.

Thermal analysis

Crystallization studies were performed on a Netzsch DSC 204 (Netzsch Co., Germany) differential scanning calorimeter under constant nitrogen flow. Sample weight was maintained at low level (3–4 mg) for all measurements. All samples were first heated to 190°C, held at 190°C for 5 min, and then cooled with a rates 10°C/min to 60°C, and held at 60°C for 5 min. They were then scanned from 60 to 190°C at a rate of 10°C.

Transmission electron microscopy

TEM observations were carried out with an H-7100 (Tokyo, Japan) instrument with an accelerating voltage of 100 kV. The ultra thin sections with a thickness of 100 nm were microtomed at 20°C by a Reichert Ultracut cryoultramicrotome without staining.

Wide-angle X-ray diffraction

WAXD spectra were recorded with a Philip X'pert prd diffractometer (Japan). The X-ray beam was nickel-filtered Cu Ka (λ = 0.1542 nm) radiation operated at 40 kV and 100 mA. OM or MP was studied as powders. Samples of UHMWPE/PP/MP composites were cut from 1 mm plates. The scanning range was varied from $2\theta = 1°$ to 50° with a rate of 5°/min.

Rheological experiments

The rheological measurements were carried out on a Gottfert Rheograph 2002 (Gottfert Co., Germany). The capillary diameter and its length-to-diameter

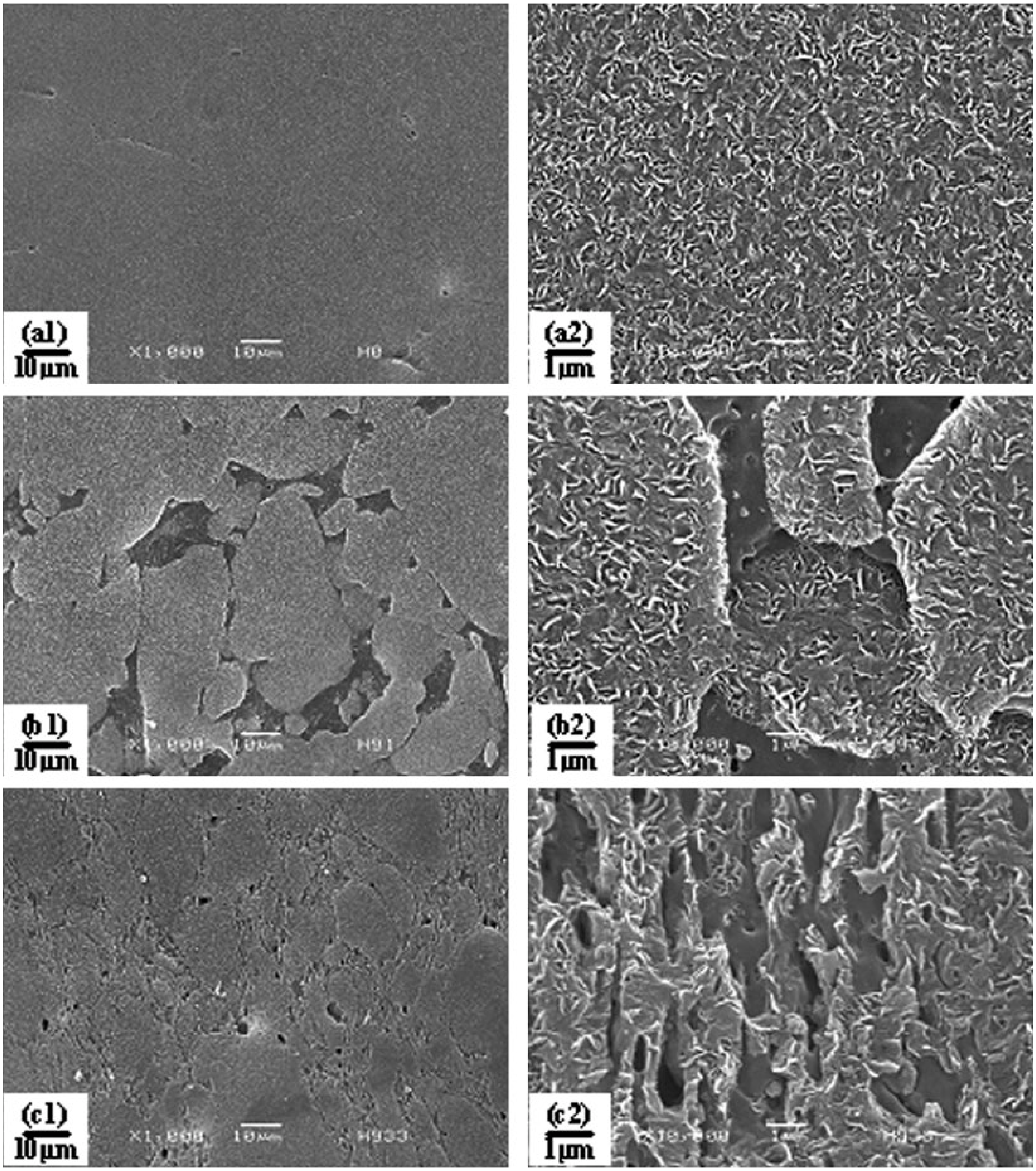

Figure 1 SEM micrographs of cryogenically fractured surfaces after etching: (a1) and (a2) pure UHMWPE; (b1) and (b2) UHMWPE/PP (90/10); (c1) and (c2) UHMWPE/PP/MP11 (90/10/3).

ratio were 1 and 30 mm, respectively. The die had an entrance angle of 180°. Entrance pressure losses were assumed to be negligible for such a long capillary die, and therefore no Bagley correction was applied. The flow properties of these specimens were measured at 200°C.

Polarizing optical microscopy

Polarized optical micrographs were taken on a Leitz Laborlux 12POL (Leitz Co., Germany) at 50× magnification. Samples were prepared through cutting small pieces from prepared films. Samples weighing

25 mg were melted on glass slides with cover slips to form thin films that were ~ 20–50 μm thick.

Scanning electron microscope

A JSM 5900 LV scanning electron microscope (Tokyo, Japan) was used to observe the morphology of UHMWPE/PP blends. Before the SEM observation, the specimens were prepared by brittle fracturing under liquid nitrogen, then etching in a solution of 1.3 wt % $KMnO_4$ dissolved in a $H_2SO_4/H_3PO_4/H_2O$ (10/4/1) mixture to eliminate the amorphous phase.

RESULTS AND DISCUSSION

Phase structure of UHMWPE/PP blends

Figure 1 shows morphology of UHMWPE, UHMWPE/PP(90/10) blends and UHMWPE/PP/MP(90/10/3) composites after etching of the amorphous phase. Pure UHMWPE displays characteristic fibril-like crystal morphology [Fig. 1(a1,a2)]. In UHMWPE/PP(90/10) blends, the morphology of the etched specimens shows an abundance of blocks, as shown in Figure 1(b1,b2). By careful observation it was determined that the dispersed blocks exhibit morphology similar to that of pure UHMWPE. It was concluded that these dispersed blocks are the crystal domains of UHMWPE, and the tangled UHMWPE can be divided into many blocks by PP in UHMWPE/PP(90/10) blends. When 3 phr MP11 was added into UHMWPE/PP (90/10) blends, the size of the dispersed blocks and the gaps between the blocks decreased and the numbers of the blocks increased.

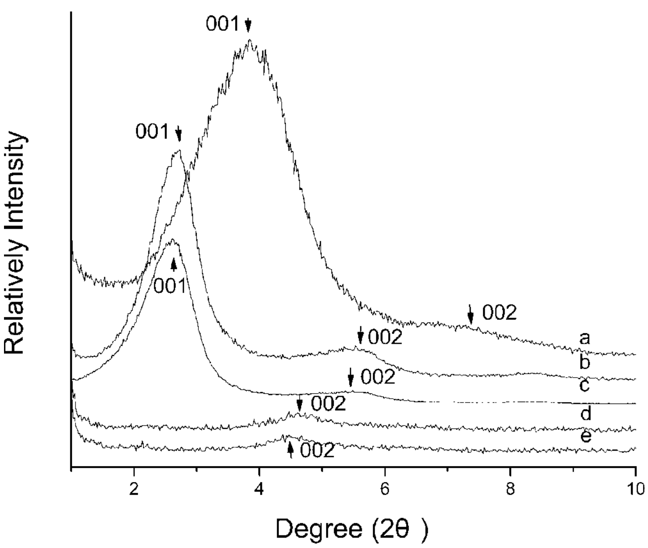

Figure 2 Wide-angle X-ray diffraction patterns of (a) OM and various composites. (b) MP21, (c) MP11, (d) UHMWPE/PP/MP21 (90/10/3), and (e) UHMWPE/PP/MP11 (90/10/3).

TABLE I
(001) Diffraction Peaks and Corresponding *d*-Spacing of OM and Various Composites

Samples	(001) 2θ	(001) *d*-Spacing
OM	3.85	2.29
MP11	2.61	3.39
MP21	2.73	3.22
UHMWPE/PP/MP11(90/10/3)	No peak	Exfoliated
UHMWPE/PP/MP21(90/10/3)	No peak	Exfoliated

The dispersion of the OM in the UHMWPE/PP/MP composites

Figure 2 compares the WAXD patterns of MP21, MP11, UHMWPE/PP/MP21 (90/10/3), UHMWPE/PP/MP11 (90/10/3), and OM. The mean interlayer spacing of the (001) plane ($d_{(001)}$) for the OM sample estimated by Bragg's formula $n\lambda = 2d\sin\theta$ is 2.29 nm ($2\theta \approx 3.85°$) [Fig. 2(a)]. The identification of the (001) diffraction peaks is summarized for all investigated samples in Table I.

As it is shown in Figure 2 and Table I, the peaks of (001) plane shifted to lower angles in both MP11 and MP21, and the peak of (001) plane disappeared in UHMWPE/PP/MP11 and UHMWPE/PP/MP21. The shifts established the formation of exfoliated and intercalated structure for UHMWPE/PP/MP, as opposed to an intercalated structure for MP systems. Figure 2 and Table I also indicate that the *d*-spacing of MP11 is larger than that of MP21.

Figure 3 shows the transmission electron micrographs of UHMWPE/PP/MP11 (90/10/3), UHMWPE/PP/MP21 (90/10/3), MP11, and MP21. As can be seen in Figure 3(a2,b2), apart from intercalated OM, well dispersed layers are also present in UHMWPE/PP/MP11 (90/10/3) and UHMWPE/PP/MP21 (90/10/3). But only the intercalated structure was able to be observed in MP11 and MP21 [Fig. 3(c,d)]. All the observations from Figure 3 are well consistent with WAXD results.

Aranda and Greeland have found that polymers containing the groups capable of associative interactions, such as hydrogen bonding, lead to intercalation.[11,12] FTIR spectra for OM is given in Figure 4, in which the absorption band at ~ 3432.50 cm^{-1} represents the hydroxyl (—OH) group. The driving force of the intercalation originates from the strong hydrogen bonding between the oxygen groups of PEG and hydroxyl groups from OM.

The intercalated PEG chains improve the interaction of OM and UHMWPE (or PP), producing the intercalated and exfoliated OM in the matrix [Figs. 2(d,e) and 3(a2)]. Additively, the surface modifier for OM lowers the surface energy of the inorganic host and converts the normally hydrophilic silicate surface to an

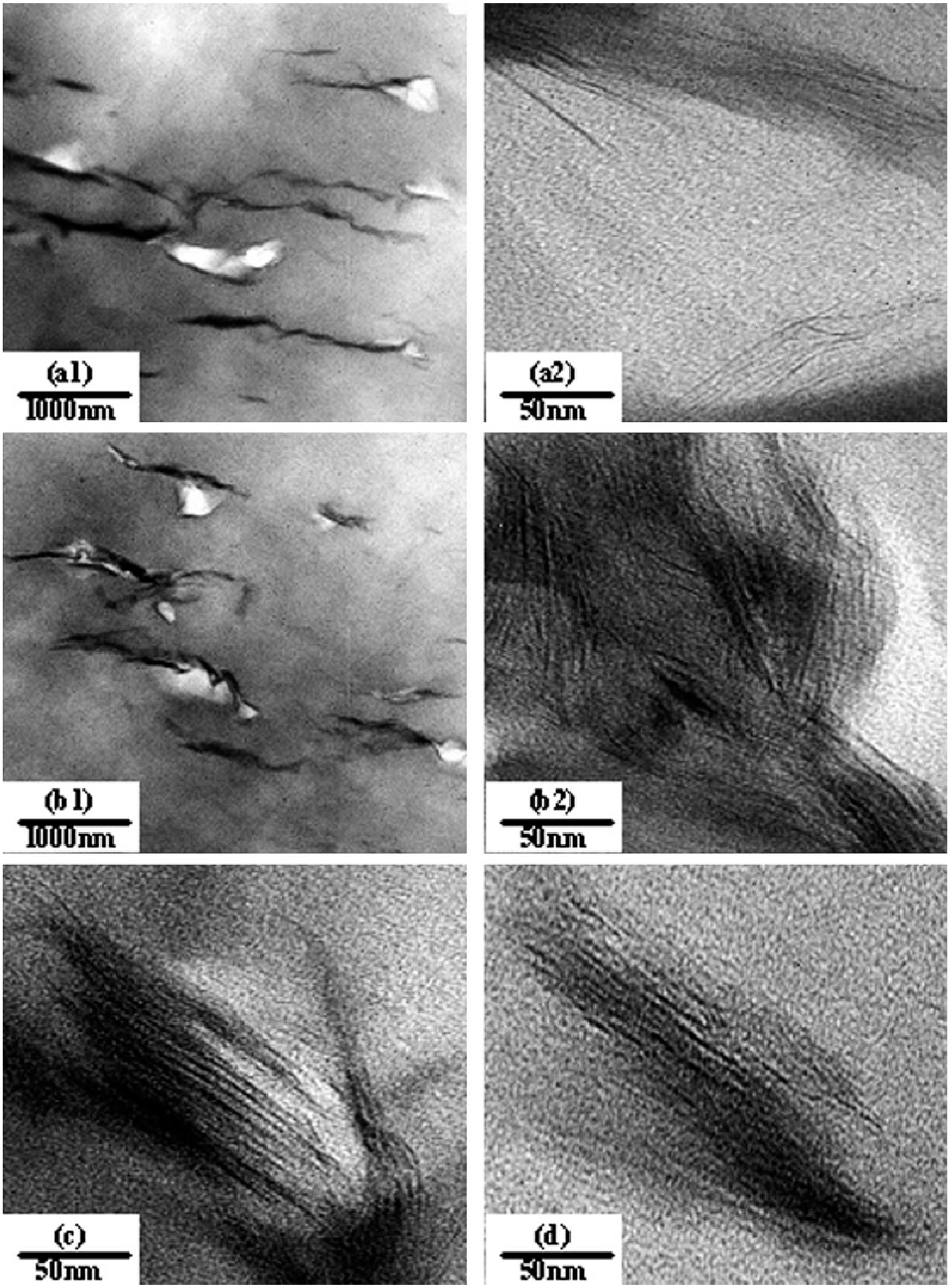

Figure 3 Transmission electron micrographs of (a1) and (a2) UHMWPE/PP/MP11 (90/10/3), (b1) and (b2) UHMWPE/PP/MP21 (90/10/3), (c) MP11, and (d) MP21.

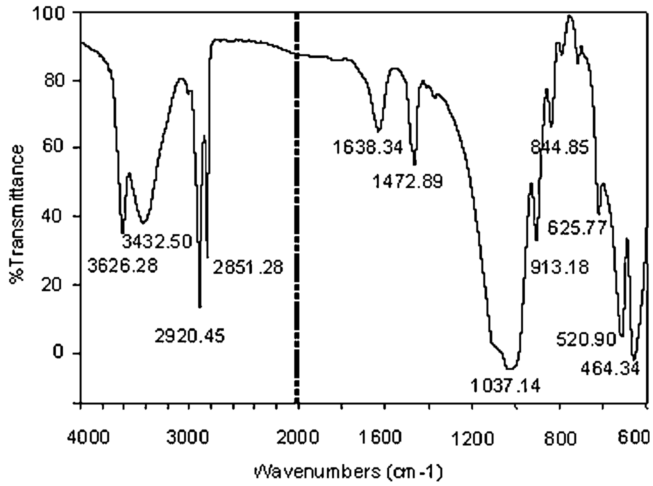

Figure 4 FTIR spectra for OM.

organophilic one, making the intercalation and exfoliation of OM possible.

Analysis of phase structure formation

Premphet and Horanont showed that in filled blends with two immiscible polymers the filler distributed selectively in the polymer-phase with which it had the lowest interfacial tension.[13] An extension of this qualitative approach has been provided by Sumita et al.[14] They introduced a wetting coefficient, W_a, which allows predicting the selectivity of filler.

$$W_a = \frac{\gamma_{\text{filler-}B} - \gamma_{\text{filler-}A}}{\gamma_{A\text{-}B}} \tag{1}$$

where $\gamma_{\text{filler-}A}$ and $\gamma_{\text{filler-}B}$ are the interfacial tensions between the fillers and polymer A or B, and $\gamma_{A\text{-}B}$ is the interfacial tension between polymer A and B. In this equation, A is PEG and B is PP or UHMWPE. If $W_a > 1$, the filler distributes within A-phase; if $-1 < W_a < 1$, the filler is located at the interface; if $W_a < -1$, the filler is selective for the B-phase.

The interfacial tensions between polymers are determined with the harmonic mean equation of Wu[15,16] [eq. (2)] where A and B are the two polymers:

$$\gamma_{AB} = \gamma_A + \gamma_B - \frac{4\gamma_A^d\gamma_B^d}{\gamma_A^d + \gamma_B^d} - \frac{4\gamma_A^p\gamma_B^p}{\gamma_A^p + \gamma_B^p} \tag{2}$$

Here γ_A and γ_B are surface tensions of the two materials in contact, and d and p superscripts denote the dispersion and polar components of the surface tensions.

For the calculation of the interfacial tensions between filler and polymers the geometric mean equation of Wu[15] [eq. (3)] is used since it is recommended for systems of a high-energy material, OM, and a low-energy material, such as the polymers used:

$$\gamma_{AB} = \gamma_A + \gamma_B - 2\left(\gamma_A^d\gamma_B^d\right)^{\frac{1}{2}} - 2\left(\gamma_A^p\gamma_B^p\right)^{\frac{1}{2}} \tag{3}$$

The corresponding values of the surface tensions at 200°C are taken from literature[15,17] and are listed in Table II. The resulting interfacial tensions for the possible pairs are given in Table III.

To apply eq. (1) to the UHMWPE/PP/PEG/OM system, we studied UHMWPE/OM/PEG and PP/OM/PEG, respectively. Table III shows that the interfacial tension between the OM and PP (or OM and UHMWPE) is by 50.4 mN/m (or 58.3 mN/m) larger than the corresponding value for the pair OM-PEG. According to Refs. 13 and 18, this indicates a large affinity of the OM to the PEG than to PP or UHMWPE in the blend. The concept of the

TABLE II
Surface Tensions at 200°C of the Polymers and Filler Used

	Surface tension (mN/m)		
Material	Total, γ	Disperse component, γ^d	Polar component, γ^p
PEG	28.5	20.4	8.1
PP	19.6	19.3	0.4
UHMWPE	26.6	26.6	0.0
OM	257.7	94.7	163.0

TABLE III
Interfacial Tensions ($\gamma_{A\text{-}B}$) and Wetting Coefficients (W_a) of All Possible Polymer–Polymer- and Polymer–Filler-Pairs

System	Possible pairs	$\gamma_{A\text{-}B}$ (mN/m)	W_a	Final phase structure
UHMWPE/OM/PEG	PEG/OM	125.6	7.1	Encapsulation
	PP/OM	176.0		
	UHMWPE/OM	183.9		
PP/OM/PEG	PP/PEG	7.1	6.6	Encapsulation
	UHMWPE/PEG	8.9		

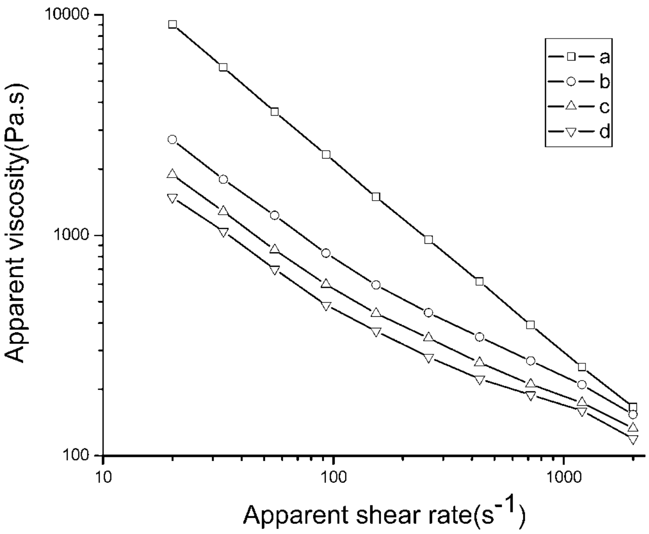

Figure 5 Plot of the logarithm of the apparent viscosity versus the logarithm of the apparent shear rate for (a) UHMWPE/PP (90/10), (b) UHMWPE/PP/MP11 (90/10/1), (c) UHMWPE/PP/MP11 (90/10/3), and (d) UHMWPE/PP/MP11 (90/10/5).

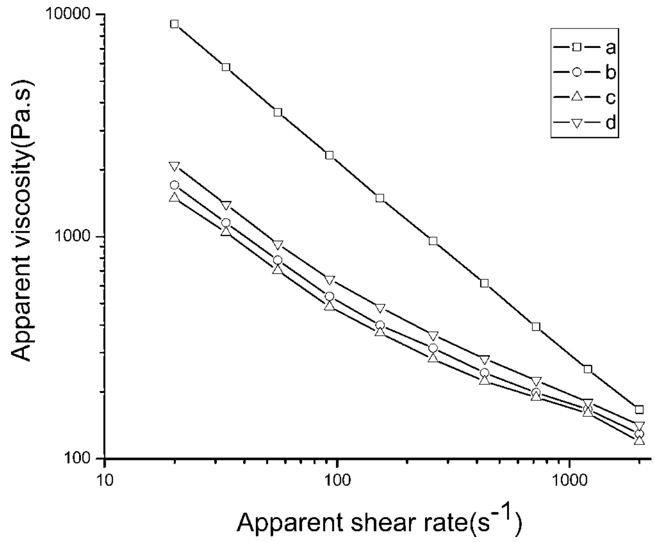

Figure 6 Plot of the logarithm of the apparent viscosity versus the logarithm of the apparent shear rate for (a) UHMWPE/PP (90/10), (b) UHMWPE/PP/MP21 (90/10/3), (c) UHMWPE/PP/MP11(90/10/3), and (d) UHMWPE/PP/MP12 (90/10/3).

wetting coefficient also confirms this tendency: eq. (1) yields wetting coefficients of 7.1 and 6.6 in PP/OM/PEG and UHMWPE/OM/PEG system, respectively. Consequently, in the extrusion of the UHMWPE/PP/MP system, PEG molecules still covered on OM layers, instead of being replaced by PP or UHMWPE molecules. Hence, an encapsulation structure of MP was finally found in the UHMWPE/PP/MP composites.

Rheological behaviors

The effect of MP and PP on the rheological properties of UHMWPE was investigated, as is shown in Figures 5–7. The melts of pure UHMWPE flew unsteadily at lower shear rate, and no steady rheology data could be obtained at higher shear rates because of the pressure vibration. Figure 5 shows that the addition of MP reduced the apparent viscosity of UHMWPE/PP (90/10) blend in the whole shear rate range investigated. With more addition of MP, more viscosity reduction of UHMWPE/PP occurred. When 1, 3, or 5 phr MP11 was added, the apparent viscosity decreased to 30, 21, and 16%, respectively, (Fig. 5). A comparison of the flow behavior of UHMWPE/PP/MP12 (90/10/3), UHMWPE/PP/MP11 (90/10/3), and UHMWPE/PP/MP21 (90/10/3) shows that the effect of the rate of (MMT : PEG) on the viscosity reduction of UHMWPE is significant and the most obvious effect occurs in UHMWPE/PP/MP11 (90/10/3) (Fig. 6).

With 5 wt % PP and 3 wt % MP11 contents in the UHMWPE/PP/MP11 composites, the apparent melt viscosity was much lower than that of pure UHMWPE, and no pressure vibration occurred throughout the whole range of shear rate [Fig. 7(a)]. Moreover, as the PP content in the blends increased, the melt apparent viscosity of UHMWPE/PP blends decreased (Fig. 7).

It is well known that PEG has very low viscosity and good lubricating property, and PEG is incompatible with UHMWPE and PP. Intercalated and exfoliated OM layers serve as a lubricant carrier in the composite. In other words, the short PEG chains

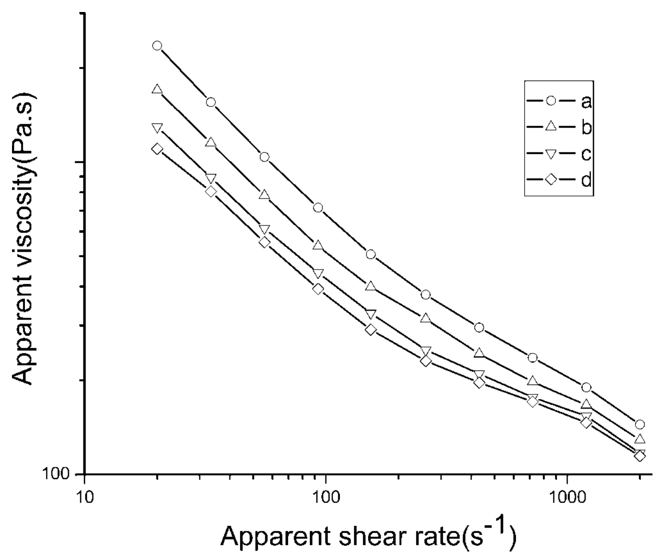

Figure 7 Plot of the logarithm of the apparent viscosity versus the logarithm of the apparent shear rate for (a) UHMWPE/PP/MP11 (95/5/3), (b) UHMWPE/PP/MP11 (90/10/3), (c) UHMWPE/PP/MP11(80/20/3), and (d) UHMWPE/PP/MP11 (70/30/3).

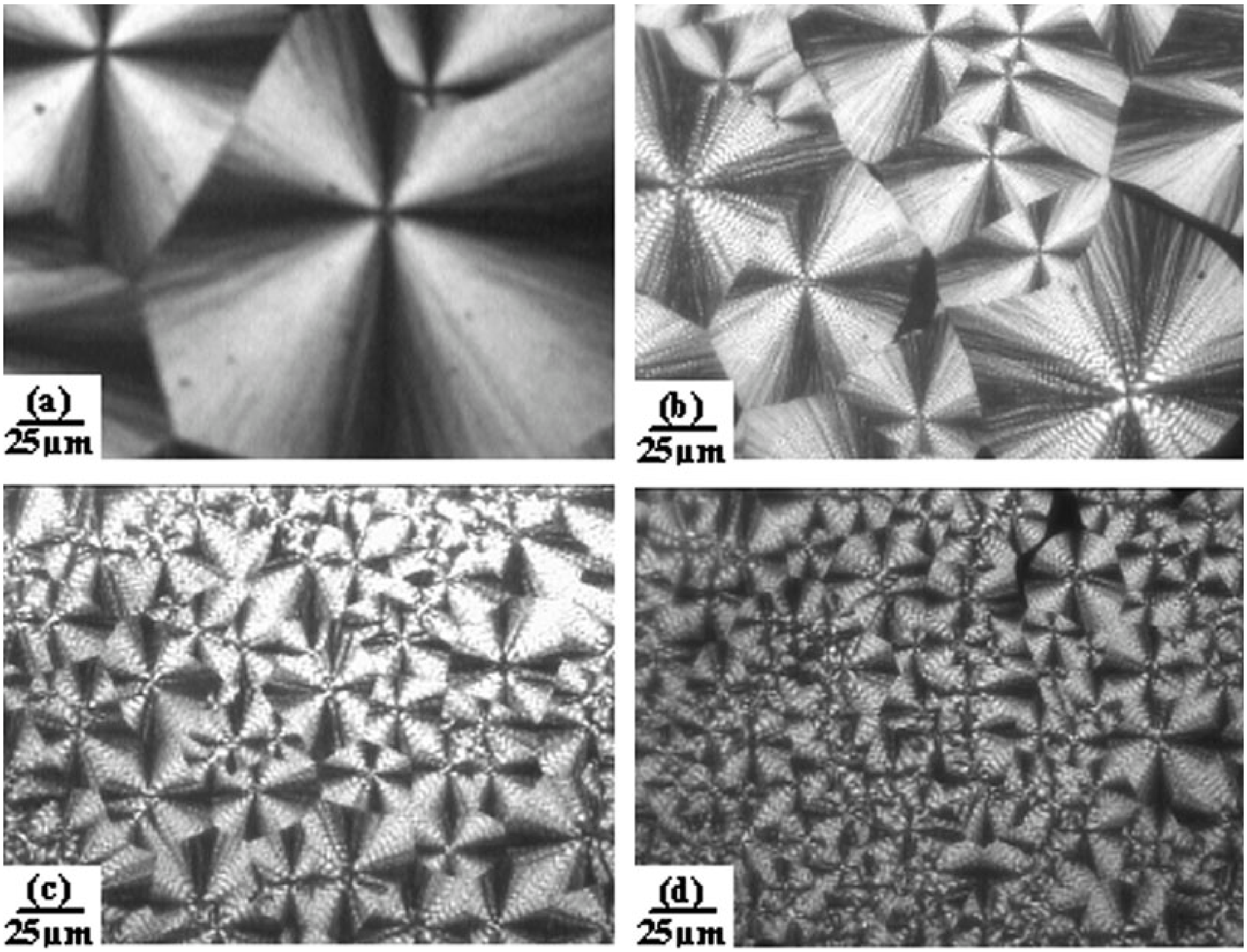

Figure 8 Optical micrographs of pure (a) UHMWPE, (b) UHMWPE/PP (90/10), (c) UHMWPE/PP/MP11 (90/10/3), (d) UHMWPE/PP/MP11 (90/10/5).

on the surface of OM can act as an internal lubricant to induce interphase slippage of the blend. Finally, synergistic effect of PEG and OM on reducing the viscosity is achieved.

Crystal structure and crystallinity

Figure 8 shows the typical spherulitic texture of UHMWPE and composites. In the case of UHMWPE, UHMWPE/PP (90/10), UHMWPE/PP/MP11 (90/10/3), and UHMWPE/PP/MP11 (90/10/5), the corresponding diameters of spherulites are about 169, 89, 53, and 28 µm. Obviously, the spherulite size gradually decreases with increasing OM content. The dispersed clay particles act as a nucleating agent, which is evident from the increase in the number density of nuclei causing smaller spherulites formation.

A series of representative endotherm curves for UHMWPE and composites were shown in Figure 9 and the corresponding values are listed in Table IV. The crystallinity of samples, $\Delta\chi_c$, can be calculated by eq. (4) (Ref. 19).

$$\Delta\chi_c = \frac{\Delta H_m}{(1-\phi)\Delta H_m^*} \times 100\% \tag{4}$$

where ϕ is the weight fraction of the filler (specifically, MP and PP in present discussion) in composite, ΔH_m is the heat fusion, ΔH_m^* denotes heat of fusion for an infinitely large crystal. ΔH_m^* of UHMWPE was measured by Wunderlich and Cormier and it was reported to be 293.0 J/g.[20]

Figure 9 and Table IV shows that crystallinity of UHMWPE in UHMWPE/PP blends tends to decrease with increasing PP ratios. In the case of pure UHMWPE, UHMWPE/PP (90/10) and UHMWPE/PP (70/30) blends, the corresponding crystallinities were 56.8, 53.2, and 52.0%. However, when 1 and 3 phr MP11 was used, the crystallinity of UHMWPE in the UHMWPE/PP (90/10) blends increased to 53.5 and 56.1%, respectively. When

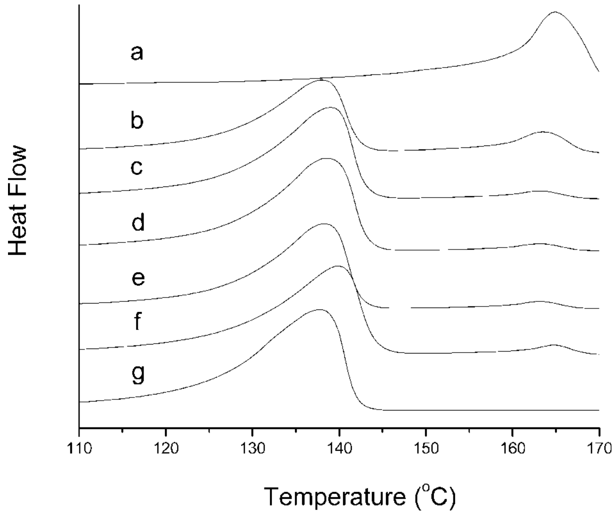

Figure 9 DSC curves of (a) PP, (b) UHMWPE/PP (70/30), (c) UHMWPE/PP/MP11 (90/10/5), (d) UHMWPE/PP/MP11 (90/10/3), (e) UHMWPE/PP/MP11 (90/10/1), (f) UHMWPE/PP (90/10), (g) UHMWPE.

5 phr MP11 was added, the crystallinity of UHMWPE decreased to 50.6% (Table IV).

Mechanical properties

Table V summarizes the mechanical properties of UHMWPE, UHMWPE/PP, and UHMWPE/PP/MP11. The stress–strain curves for the samples are similar. In the case of UHMWPE/PP(90/10) blend, its mechanical properties remain nearly unchanged when compared with pure UHMWPE. But apparent enhancement of tensile strength, elongation at break, and Young's modulus of UHMWPE/PP(90/10) blend appeared when 1, 3, and 5 phr MP11 were respectively, added into it, except that Izod-notched impact strength was without much obvious change. Especially when 3 phr of MP11 was added, a 28.3% increase in tensile strength, 17.0% increase in Elongation at break, and 35.8% increase in Young' modulus were observed. The mechanical properties enhanced as a result of the decrease of defects at boundaries between UHMWPE spherulites because of the role of MP11 as nucleating agent.

TABLE IV
DSC Analysis of Pure UHMWPE, UHMWPE/PP, and UHMWPE/PP/MP11

Sample	UHMWPE		
	T_m	ΔH_m	$\Delta\chi_c$
UHMWPE	137.8	166.4	56.8
UHMWPE/PP(90/10)	139.9	140.3	53.2
UHMWPE/PP(70/30)	138.3	106.6	52.0
UHMWPE/PP/MP11(90/10/1)	139.1	137.9	53.5
UHMWPE/PP/MP11(90/10/3)	138.7	144.6	56.1
UHMWPE/PP/MP11(90/10/5)	138.4	126.0	50.6

TABLE V
The Mechanical Properties of Pure UHMWPE, UHMWPE/PP, and UHMWPE/PP/MP11

Sample	Tensile strength (MPa)	Elongation at break (%)	Young's modulus (MPa)	Izod-notched impact strength (kJ/m^2)
UHMWPE	36.0	393.4	740.2	No break
UHMWPE/PP(90/10)	37.9	401.2	750.2	No break
UHMWPE/PP/MP11(90/10/1)	39.2	413.1	876.3	No break
UHMWPE/PP/MP11(90/10/3)	46.2	460.1	1005.0	No break
UHMWPE/PP/MP11(90/10/5)	39.7	428.2	1027.0	No break

CONCLUSIONS

The WAXD analysis and TEM observation clearly indicate the intercalation and exfoliation structure of OM in UHMEPE/PP/MP. The extent of dispersion depends on the hybrids (OM/PEG) weight ratio and the dispersion is best when PEG : OM ratio is 1 : 1.

The addition of a small amount of MP11 has been found able to reduce the melt viscosity of UHMWPE/PP (90/10) blend significantly. With 1 wt % MP11 contents in UHMWPE/PP (90/10) blend, the apparent melt viscosity is much lower than that of pure UHMWPE, and no pressure vibration occurs throughout the whole range of shear rate. With more addition of MP11, more viscosity reduction of UHMWPE/PP (90/10) occurs.

The UHMWPE/PP/MP11 (90/10/3) composite has the optimum comprehensive mechanical property. When the amount of MP11 is 1 or 5%, properties such as tensile strength and elongation at break of composites decrease, but they are still higher than those of the pure UHMWPE and UHMWPE/PP blend.

References

1. Lemstra, P. J.; Kirschbaum, R. Polymer 1985, 26, 1372.
2. Barham, P. J.; Keller, A. J Mater Sci 1985, 20, 2281.
3. Vaia, R. A.; Ishii, H.; Giannelis, E. P. Chem Mater 1993, 5, 1694.
4. Kato, M.; Usuki, A.; Okada, A. J Appl Polym Sci 1997, 66, 1781.
5. Park, J. H.; Jana, S. C. Macromolecules 2003, 36, 2758.
6. Reichert, P.; Nitz, H.; Klinke, S.; Brandsch, R.; Thomann, R.; Mulhaupt, R. Macromol Mater Eng 2000, 375, 8.
7. Kawasumi, M.; Hasegawa, N.; Kato, M.; Okada, A. Macromolecules 1997, 30, 6333.
8. Vaia, R. A.; Jandt, K. D.; Kramer, E. J.; Giannelis, E. P. Macromolecules 1995, 28, 8080.

9. Reichert, P.; Hoffmann, B.; Bock, T.; Thomann, R.; Mülhaupt, R.; Friedrich, C. Macromol Rapid Commun 2001, 22, 519.
10. Kharchenko, S. B.; Douglas, J. F.; Obrzut, J.; Grulke, E. A.; Migler, K. B. Nat Mater 2004, 3, 564.
11. Aranda, P. Chem Mater 1992, 4, 1395.
12. Greeland, D. J. J Colloid Sci 1963, 18, 647.
13. Premphet, K.; Horanont, P. Polymer 2000, 41, 9283.
14. Sumita, M.; Sakata, K.; Asai, S.; Miyasaka, K.; Nakagawa, H. Polym Bull 1991, 25, 265.
15. Wu, S. Polymer Interface and Adhesion; Marcel Dekker: New York, 1982.
16. Wu, S. Polym Eng Sci 1987, 27, 335.
17. Pukanszky, B.; Fekete, E. Adv Polym Sci 1999, 139, 109.
18. Schuster, R. H.; Issel, H. M.; Peterseim, V. I. Rubber Chem Technol 1996, 69, 769.
19. Krikorian, V.; Pochan, D. J. Macromolecules 2004, 37, 6480.
20. Wunderlich, B.; Cormier, C. M. J Polym Sci Polym Phys Ed 1967, 5, 987.